

Influence of biomass burning plumes on HONO chemistry in eastern China

W. Nie^{1,2}, A. J. Ding^{1,2}, Y. N. Xie^{1,2}, Z. Xu³, H. Mao^{1,2,5}, V. Kerminen⁴, L. F. Zheng^{3,1}, X. M. Qi^{1,2}, X. Huang¹, X. Q. Yang^{1,2}, J. N. Sun^{1,2}, E. Herrmann¹, T. Petäjä⁴, M. Kulmala⁴ and C. B. Fu^{1,2}

¹Institute for Climate and Global Change Research & School of Atmospheric Sciences, Nanjing University, Nanjing, 210093, China

²Collaborative Innovation Center of Climate Change, Jiangsu Province, China

³Environment Research Institute, Shandong University, Jinan, China

⁴Division of Atmospheric Sciences, Department of Physics, University of Helsinki, Helsinki, Finland

⁵Department of Chemistry, State University of New York College of Environmental Science and Forestry, Syracuse, New York, USA

1 **Abstract.** Nitrous acid (HONO) plays a key role in atmospheric chemistry via
2 influencing the budget of hydroxyl radical (OH). In this study, a two-month
3 measurement of HONO and related quantities were analyzed during a biomass
4 burning season in 2012 at a suburban site in the western Yangtze River delta, eastern
5 China. An overall high HONO concentration with the mean value of 0.76 ppbv (0.01
6 ppbv to 5.95 ppbv) was observed. During biomass burning (BB) periods, both HONO
7 concentration and HONO/NO₂ ratio were enhanced significantly (more than a factor
8 of 2, $p < 0.01$) compared with non-biomass burning (Non-BB) periods. A correlation
9 analysis showed that the HONO in BB plumes was more correlated with nitrogen
10 dioxide (NO₂) than that with potassium (a tracer of BB). Estimation by the method of
11 potassium tracer suggests a maximum contribution of $17\% \pm 12\%$ from BB emission
12 to the observed HONO concentrations, and the other over 80% of the observed
13 nighttime HONO concentrations during BB periods were secondarily produced by the
14 heterogeneous conversion of NO₂. The NO₂-to-HONO conversion rate (C_{HONO}) in BB

15 plumes was almost twice as that in non-BB plumes (0.0062 hr^{-1} vs 0.0032 hr^{-1}). Given
16 the residence time of the BB air masses was lower than that of non-BB air masses,
17 these results suggest BB aerosols have higher NO_2 conversion potentials to form
18 HONO than non-BB aerosols. A further analysis based on comparing the surface area
19 at similar particle mass levels and HONO/ NO_2 ratios at similar surface area levels
20 suggested larger specific surface areas and higher NO_2 conversion efficiencies of BB
21 aerosols. A mixed plume of BB and anthropogenic fossil fuel (FF) emissions was
22 observed on 10 June with even higher HONO concentrations and HONO/ NO_2 ratios.
23 The strong HONO production potential (high HONO/ NO_2 to $\text{PM}_{2.5}$ ratio) was
24 accompanied with a high sulfate concentration in this plume, suggesting a promotion
25 of mixed aerosols to the HONO formation. In summary, our study suggests an
26 important role of BB in atmospheric chemistry by affecting the HONO budget. This
27 can be especially important in eastern China, where agricultural burning plumes are
28 inevitably mixed with urban pollutions.

29 **1. Introduction**

30 Nitrous acid (HONO) is an important constituent in the troposphere due to its role in
31 hydrogen oxides (HO_x) cycling (Platt et al., 1980; Kleffmann, 2007; Hofzumahaus et
32 al., 2009; Elshorbany et al., 2012). The photolysis of HONO provides a daytime
33 source of hydroxyl radical (OH), which controls the daytime oxidation capacity and
34 consequently influences the ozone (O_3) chemistry and secondary organic aerosol
35 (SOA) formation. This process is especially important in the early morning when
36 contributions from other OH sources, like O_3 photolysis, are still small (Alicke et al.,
37 2002; Kleffmann et al., 2005; Elshorbany et al., 2010).

38 The sources of atmospheric HONO, including direct emission from fossil fuel
39 combustion (Kurtenbach et al., 2001) and soil (Su et al., 2011), homogeneous gas
40 phase reactions and heterogeneous processes on the surface of atmospheric aerosols
41 and ground (Harrison and Collins, 1998; Longfellow et al., 1999; Stutz et al., 2002;
42 VandenBoer et al., 2013), are hitherto not well understood. Among these sources,

43 heterogeneous processes are commonly accepted as the least understood pathway to
44 produce HONO. For example, [nitrogen dioxide \(NO₂\)](#) can be converted to HONO on
45 ground (Harrison and Kitto, 1994), wet surfaces (Finlayson-Pitts et al., 2003), soot
46 particles (Ammann et al., 1998; Kalberer et al., 1999; Kleffmann and Wiesen, 2005),
47 and organic substrates (Bröske et al., 2003; Ammann et al., 2005). These processes
48 have been considered as the primary contributor to the nocturnal HONO formation,
49 but they cannot sustain the frequently-observed elevated daytime HONO
50 concentration levels (Kleffmann, 2007; Sörgel et al., 2011; Li et al., 2012, and the
51 references there in). Recently, several heterogeneous and possibly photo-enhanced
52 processes have been demonstrated that might play an important role in daytime
53 HONO formation (George et al., 2005; Stemmler et al., 2006; Ndour et al., 2008; Nie
54 et al., 2012; Langridge et al., 2009; Bedjanian and El Zein, 2012). However, although
55 these studies have drawn a clearer picture on the HONO chemistry, there are still
56 large knowledge gaps in HONO sources. [The heterogeneous production of HONO in
57 the atmosphere by the mechanistic variety is still under debate.](#)

58 Biomass burning is a major source of atmospheric aerosol particles (Janhäll et al.,
59 2010) and trace gases (Andreae and Merlet, 2001; Burling et al., 2010), consequently
60 influencing climate and air quality. Recent studies have connected the HONO
61 chemistry to biomass burning via both direct HONO emissions and emissions of soot
62 particles (Roberts et al., 2010; Veres et al., 2010). Although high emission ratios of
63 HONO have been detected in the laboratory fires (Burling et al., 2010; Veres et al.,
64 2010), the mixing ratio of HONO in aged biomass burning plumes is expected to be
65 relatively independent of its direct emissions due to the rapid dilution and [photolysis](#)
66 for primary HONO during the atmospheric transport. Soot particles, as one major
67 component in biomass burning plumes, have been demonstrated to be an effective
68 media to convert NO₂ to HONO (Kleffmann et al., 1999; Aumont et al., 1999; Prince
69 et al., 2002; Kleffmann and Wiesen, 2005; Aubin and Abbatt, 2007), especially in the
70 case that aged soot particles can be re-activated in the present of light (Monge et al.,
71 2010) and play a continuous role in the HONO chemistry. These processes may

72 significantly influence the HONO chemistry during a biomass burning period, but
73 their exact roles are rarely demonstrated in the real atmosphere, especially when BB
74 aerosols are mixed with anthropogenic pollutants.

75 In this study, a two-month measurement campaign was conducted during the intensive
76 BB (burning of wheat straw) period (April to June 2012) at the SORPES station
77 (Stations for Observing Regional Processes of the Earth System) in western Yangtze
78 River delta (YRD) of East China (Ding et al., 2013c). Several HONO-related
79 quantities were measured, with the aim to investigate the HONO chemistry in YRD, a
80 region undergoing rapid urbanization and industrialization. A special attention was
81 paid to the impact of BB plumes and mixed plumes of agricultural burning and fossil
82 fuel (FF) emissions on HONO formation after a long-range transport. In the following,
83 the general features related to HONO during the campaign were first described. The
84 differences in HONO formation between the BB events and non-BB events were then
85 be investigated. The influences of mixed plumes of intensive BB and FF emission
86 (Ding et al., 2013b) on HONO formation were finally discussed.

87 **2. Experimental methodologies**

88 **2.1 Field campaign**

89 The field campaign was conducted from late April to June 2012 at the SORPES
90 “flagship” central site in Xianlin (Ding et al., 2013c). It is a regional background site,
91 located on the top of a hill (118°57'10" E, 32°07'14", 40 m a.s.l.) in the Xianlin
92 campus of Nanjing University and about 20 km east of the suburban Nanjing city (See
93 Fig. 1 in Ding et al., 2013c). A suite of trace gases, aerosols and meteorological
94 quantities were measured, with more detailed descriptions found in Ding et al.
95 (2013b). The present study is focused on HONO and related quantities, including NO₂,
96 NO_x, CO, SO₂, PM_{2.5} mass, total water-soluble ions (WSIs), potassium ions (K⁺),
97 sulfate (SO₄²⁻), and particle surface-area size distribution over the size range of 6–800
98 nm.

99 2.2 Measurement techniques

100 The HONO concentration was measured with a Monitor for Aerosols and Gases in
101 Air (MARGA, Metrohm Co.), which includes a wet rotating denuder (WRD)
102 (Spindler et al., 2003; Su et al., 2008; Makkonen et al., 2012) connected to an ion
103 chromatograph (IC, Metrohm USA, Inc., Riverview, FL). The time resolution of this
104 measurement is 1 h. There were 1608 hourly samples during the campaign. The WRD
105 consists of two concentric glass cylinders whose wall is coated with 10 ppm H₂O₂
106 solution to absorb HONO and other gases. The liquid sample streams from WRD are
107 drawn into 25 ml syringes before being injected into the IC system. The residence
108 time of sampling air is about 4.5 s in the sampling tubes and about 0.2 s in WRD.

109 Other measurement techniques are described briefly as follows. The fine particle mass
110 concentration (PM_{2.5}) was continuously measured with a combined technique of light
111 scattering photometry and beta radiation attenuation (Thermo Scientific SHARP
112 Monitor Model 5030). Sulfate (SO₄²⁻) and potassium ions (K⁺) concentrations in
113 PM_{2.5} were measured with the MARGA system (Ding et al., 2013b). NO₂ was
114 converted to nitric oxide (NO) with a molybdenum oxide (MoO) catalytic converter
115 inside the instrument and measured with a chemiluminescence analyzer (TEI model
116 42i). It should be noted that the technique of molybdenum converter to measure NO₂
117 may overestimate its ambient concentrations at daytime due to the potential
118 conversion of species other than NO₂ (e.g. peroxyacetyl nitrate (PAN)) to NO (Xu et
119 al., 2013). But the interference is much lower at nighttime without photochemical
120 reaction. Total reactive nitrogen oxides (NO_y) was measured with an externally placed
121 molybdenum converter and a NO analyzer. The sulfur dioxides (SO₂) concentration
122 was measured with a pulsed UV fluorescence analyzer (TEI model 43i). Detailed
123 information can be found in Ding et al. (2013b).

124 2.3 Sampling artifacts and data correction

125 The sampling artifacts of HONO measurement with WRD method are mainly caused
126 by the NO₂ conversion on the surface of the sampling tube and WRD (interference 1)

127 and the reaction of NO₂ with S (IV) in the absorption solution in WRD (interference 2)
128 (Spindler et al., 2003; Barnes and Rudziński, 2012). In this study, 10 ppm of H₂O₂
129 was used as the absorption solution for the MARGA system, which can oxidize the S
130 (IV) very quickly to form H₂SO₄, and thus can avoid the interference 2 induced by the
131 reaction of NO₂ with S (IV) (Genfa et al., 2003). In addition, the formation of H₂SO₄
132 can acidize the absorption solution, which will reduce the interference 1 in WRD by
133 suppressing the absorption and reaction of NO₂ on the surface of the absorption
134 solution (Kleffmann et al., 2002). Therefore, in this study, the interference of HONO
135 measurement should be mainly from the NO₂ conversion on the surface of the
136 sampling tube (part of interference 1). Here, to avoid the possible overestimation, we
137 corrected the dataset with the following formula recommended by an
138 inter-comparison study on the HONO measurement between a WRD and a LOPAP
139 system conducted in a similar atmospheric environment in China (Su, 2008):

$$140 \text{HONO}_{\text{LOPAP}} = 0.833 * \text{HONO}_{\text{WRD}} - 0.17$$

141 It should be noted that the dataset corrected by this formula is expected to
142 underestimate the HONO concentration because the absorption solution deployed by
143 Su (2008) was Na₂CO₃, which can induce additional interference in WRD
144 (interference 2 and part of interference 1). Given that we probably underestimated the
145 HONO concentrations and overestimated the NO₂ concentrations (Xu et al., 2013),
146 the values of HONO/NO₂ and HONO/NO_x calculated in section 3 are actually lower
147 limits for these ratios.

148 Several studies (Appel et al., 1990; Th. Muller, 1999; Genfa et al., 2003) [have](#)
149 [demonstrated that the overestimation of HONO concentrations measured by WRD are](#)
150 [mainly occurred during daytime, so we used only](#) nighttime data (except the case of
151 10 June, when the solar radiation was significantly decreased to a very low level
152 (Ding et al., 2013b).) in sections 3.2 and 3.3.

153 **2.4 Calculation of the nocturnal HONO lifetime**

154 Generally the nocturnal boundary layer is low and stable, the observed plumes during
 155 the nighttime were assumed to always be transported inside the boundary layer and
 156 probably contact to the ground surface. In this case, there are three major pathways
 157 for the loss of HONO during nighttime, including deposition on ground surfaces
 158 (Path-A), heterogeneous loss on aerosol surfaces (Path-B) and reaction with the OH
 159 radical (Path-C) (Li et al., 2012). For Path-A, the HONO lifetime (T_a) is given by

$$T_a = \frac{1}{k_a} = \frac{H}{V_{HONO}}$$

160 where H is the mixing height (assumed as 100 m) and V_{HONO} is the dry deposition
 161 velocity of HONO, assumed to be equal to 0.8 cm s^{-1} (Li et al., 2012). For the loss
 162 Path-B, the corresponding lifetime (T_b) can be written as

$$T_b = \frac{1}{k_b} = \frac{1}{\frac{1}{4} * \gamma_{HONO} S_{aerosol} * \overline{v_{HONO}}}$$

163 There is no modern literature reporting the HONO uptake coefficient on aerosol, but
 164 an uptake coefficient of HONO on the ground ranging from 10^{-5} to 10^{-4} was reported
 165 in recent studies (VandenBoer et al., 2013; Donaldson et al., 2013). Considering lower
 166 surface area and pH of aerosol (Su et al., 2011), the uptake coefficient of HONO on
 167 aerosol may be less and was estimated as 10^{-5} or less. $S_{aerosol}$ is the aerosol surface
 168 during the observation with a mean value of about $1.5 \times 10^3 \mu\text{m}^2 \text{ cm}^{-3}$ calculated from
 169 the particle size distribution, and $\overline{v_{HONO}}$ is the mean molecular velocity of HONO
 170 (about 380 m/s). For the loss Path-C, the lifetime (T_c) is equal to

$$T_c = \frac{1}{k_c} = \frac{1}{k * OH}$$

171 The OH concentration was estimated as 10^6 mol cm^{-3} (Hofzumahaus et al., 2009).
 172 $K_{HONO+OH}$ is the reaction rate of HONO and OH. The value of $5.0 \times 10^{-12} \text{ cm}^3 \text{ s}^{-1}$ at 298
 173 K (Sander et al., 2006) was used. In these conditions, the overall lifetime, T , is
 174 obtained from the following formula:

$$\frac{1}{T} = \frac{1}{T_a} + \frac{1}{T_b} + \frac{1}{T_c}$$

175 The lifetime of HONO was calculated to be about 3.3 hours. That means about 8-9
176 hours are needed to for the emitted HONO to be consumed within the nocturnal PBL.

177 **2.5 Tracer of biomass burning plumes**

178 Most BB tracers are organic matters (Simoneit, 2002; Andreae and Merlet, 2001),
179 which were not measured during this campaign. Carbon monoxide (CO) in the gas
180 phase (Andreae and Merlet, 2001) and potassium ions (K⁺) in the aerosol phase
181 (ANDREAE, 1983; Ma et al., 2003; Reid et al., 2005; Li et al., 2007) are well
182 recognized inorganic tracers of BB. In this study, the observation site is located in
183 YRD, one of the best developed and most polluted regions in China (Ding et al.,
184 2013c). Many CO sources other than BB, such as industry and traffic, can contribute a
185 lot to the CO loading even during the BB season. Instead, no other significant sources
186 of K⁺ are around this region. Therefore, K⁺ is suitable tracer of BB for the regions
187 with heavy air pollutions. In this study, the samples with K⁺ concentrations higher
188 than 2 μg m⁻³ and the ratio of K⁺ to PM_{2.5} larger than 0.02 were defined as BB
189 samples (203 samples). The samples with K⁺ concentrations lower than 2 μg m⁻³ and
190 the ratio of K⁺ to PM_{2.5} smaller than 0.02 were categorized as non-BB samples (1122
191 samples). The defined samples, including BB and non-BB samples, account for 82.4%
192 of the total samples. The other undefined samples account for 17.6%.

193 **3. Results and discussions**

194 **3.1 Observation overview**

195 Figure 1 shows the temporal variations of concentrations of HONO, NO₂, PM_{2.5} mass
196 and K⁺ observed at the Xianlin SORPES central site during the time period of April –
197 June 2012. The average concentration of HONO was 0.76 ± 0.79 ppbv, which was
198 lower than the concentrations measured at a polluted rural site in the Pearl River Delta
199 region (Su et al., 2008) and an urban site in Shanghai (Wang et al., 2013), but much

200 higher than those measured in Europe (Acker and Möller, 2007). Both HONO
201 concentrations (Fig. 2a) and ratios of HONO to NO₂ (HONO/NO₂) (Fig. 3b) both
202 exhibited distinct diurnal cycles, with a diurnal maximum during night/early morning
203 and minimum around the noon.

204 During the campaign and especially from late May to early June, several BB episodes
205 were observed and revealed by elevated concentrations of PM_{2.5} (up to 426 μg m⁻³)
206 and K⁺ (up to 22 μg m⁻³) (Fig. 1) (Ding et al., 2013b; Ding et al., 2013c). HONO
207 concentrations were also enhanced during the BB episodes. In order to investigate the
208 relation between BB and HONO chemistry, we compared the HONO concentrations,
209 HONO/NO₂ ratios and HONO/NO_x ratios between the BB and non-BB periods. On
210 average, all the three parameters were significantly enhanced during BB periods than
211 during non-BB periods (Figs. 3d-3f). HONO concentrations increased by 156% (1.56
212 ± 1.43 ppbv vs 0.61 ± 0.54 ppbv, p<0.01); HONO/NO₂ ratios increased by 137%
213 (0.066 ± 0.043 vs 0.028 ± 0.020, p<0.01); HONO/NO_x ratios increased by 134%
214 (0.055 ± 0.031 vs 0.023 ± 0.016, p<0.01). These results indicate a positive impact of
215 BB plumes on the ambient mixing ratio of HONO.

216 The enhanced HONO production in BB plumes would impact the atmospheric
217 oxidation capacity, and influence the formation of secondary aerosols (Li et al., 2010;
218 Gonçalves et al., 2012; Elshorbany et al., 2014). In this study, the average values of
219 HONO to NO_x ratios (0.028 ± 0.021), especially during the BB periods (0.062 ±
220 0.031) (see Fig. 3f) were considerably higher than 0.02, the assumed global averaged
221 value (Elshorbany et al., 2012; Elshorbany et al., 2014), suggesting a potential more
222 important role for HONO chemistry in the YRD, especially during the BB season.

223 3.2 Influence of BB on HONO formation

224 3.2.1 Contribution of direct emission

225 Several laboratory studies have demonstrated BB as an effective HONO source via
226 direct emissions (Burling et al., 2010; Veres et al., 2010), so HONO might play an

227 important role in atmospheric chemistry over BB source regions. However, HONO is
228 easily consumed by chemical sinks during its atmospheric transport (the estimated
229 lifetime was about 3.3 hours in the night time, and emitted HONO can be consumed
230 in about 8 hours, see section 2.4). In this study, the main BB source area is located in
231 the northern part of Anhui province, several hundred kilometers from the SORPES
232 station (Fig. 4). As showed in Fig. 4a, in addition to some individual fire points
233 distributed in the 8-hr backward retroplume, the air masses from the major source
234 regions cannot influence SORPES station in 8-hr transport, suggesting the direct
235 emission from BB may influence on the observed enhancement of the HONO but
236 should not be the major contributor. The correlations of HONO with K^+ (BB tracer)
237 and NO_2 for the night time BB samples were illustrated in Fig. 5 and Fig.10. The
238 results showed the HONO was positively correlated to both K^+ and NO_2 , but the
239 correlation efficiency (R) for HONO and NO_2 was higher than that for HONO and K^+ .
240 These results indicate that despite of some contribution from direction emission, the
241 secondary production of HONO should play the key role.

242 As few publications reported the emission factors of both K^+ and HONO from the
243 burning of wheat straw, here to estimate the contribution of BB direct emission to
244 HONO, we first calculated the contribution of BB emission to observed CO
245 concentrations. The ratio of emission factors of K^+ and CO was assumed to be
246 identical for the BB events observed during this campaign. Here we took the
247 minimum molar ratio of non-background CO to K^+ for night time BB samples (the
248 value was 67) as the ratio of the emission factors of these two species because of the
249 additional strong CO sources other than BB emission in YRD. The background
250 concentrations of CO around SORPES station were estimated as the intercept of the
251 linear regression fit for the whole samples of CO and NO_y during the campaign (the
252 value was 480 ppb, figure not shown) (Wang et al., 2004). In such case, the CO
253 concentration contributed from BB emission was calculated to be 260 ± 189 ppbv.

254 Then we estimated the contribution of BB emission to observed HONO
255 concentrations by taking account of the emission ratio of HONO to CO from the

256 burning of wheat straw and the loss of emitted HONO during the transport. Noting
257 that the deposition of CO and K⁺ in fine particles was slow, their losses during the
258 transport were assumed to be negligible. The averaged emission ratio of HONO to CO
259 from the burning of wheat straw was taken as 0.0027 (Stockwell et al., 2014). The
260 loss of HONO should be relative with the transport time of BB plumes. However, the
261 transport time was difficult to be calculated as the exact source region (fire point on
262 the map, Fig. 4) for each BB episode cannot be identified. Some episodes maybe
263 influenced by several source regions on the transport pathway. And the exact time and
264 duration of the fires cannot be identified with the satellite fire count data. But given
265 that there was few fire points very close to SORPES station (Fig. 4), and the air
266 plumes of several episodes, such as 9-11 June and 12-13 June, have been
267 demonstrated being transported several days before arriving the station (Fig. 9d and
268 9e in Ding et al., 2013c), we therefore used 3.3 hours (HONO nighttime lifetime, see
269 section 2.4) as the mean transport time, which were actually underestimated for most
270 BB episodes to estimate HONO loss during transportation. In such case, although
271 there may be large uncertainties, here our best estimation of HONO contribution from
272 direct emission of BB was 0.27 ± 0.19 ppbv, which accounted for $17\% \pm 12\%$ of the
273 observed HONO concentrations. That means more than 80% of the observed
274 nighttime HONO during BB periods was secondarily formed.

275 **3.2.2 Heterogeneous conversion and possible influence of ground surface**

276 Reaction of NO and OH was one major source of daytime HONO, but its contribution
277 to nighttime HONO is negligible due to the limitation of nighttime OH concentration .
278 Therefore, the over 80% of the observed HONO in the night time BB plumes, which
279 was secondary formed, should be produced from the heterogeneous conversation of
280 NO₂. In such case, the enhancement of HONO during BB periods should be ascribed
281 to either the increase in NO₂ concentrations or increased NO₂ to HONO conversion
282 potentials. As shown in Figs. 1 and 3c, the concentration levels of NO₂ were
283 comparable during the BB and non-BB periods (p=0.51), so the higher HONO level
284 during BB period was probably due in large part to a higher NO₂ conversion potential

285 (HONO/NO₂ ratio).

286 To further verify this point, in Fig. 6, we presented the changes of HONO to NO₂
287 ratios during night time for both BB and non-BB plumes. The NO₂-to-HONO
288 conversion rate (C_{HONO}), which estimated by change rates of HONO/NO₂ ratios along
289 the time (the slopes in Fig. 6, 19:00 to 03:00), in BB plumes almost 2 times higher
290 than that in non-BB plumes (0.0062 hr⁻¹ vs 0.0032 hr⁻¹), further suggesting higher
291 NO₂ conversion potential to produce HONO in BB plumes than that in non-BB
292 plumes.

293 Both ground and aerosols are effective surfaces for converting NO₂ to HONO. Here,
294 to estimate the possible role of ground surface in the enhancement of HONO
295 concentrations, we conducted backward Lagrangian dispersion modeling for the air
296 masses arriving the SORPES station using the HYSPLIT model following the method
297 developed by Ding et al., (2013a). Considering that the nighttime HONO lifetime was
298 estimated to be about 3.3 hours, we run the models for an 8-hour backward period,
299 during which the emitted HONO from BB can possibly be consumed. Figs. 4a and 4b
300 presented the "footprint" retroplumes, which represented the distribution of
301 probability or residence time of the simulated air masses in their last 8-hour transport
302 time prior to arrival at measurement site (Ding et al., 2013a). The residence time was
303 calculated to be 10% lower for BB air masses than that for Non-BB air masses,
304 suggesting the aerosol surface rather than the ground surface was the major
305 contributor to the observed enhancement of HONO concentrations and HONO/NO₂
306 ratios during BB periods. It should be noted here we cannot totally get rid of the
307 influence of ground surface as the exact role of varied land use and land cover in
308 HONO chemistry was not clear. But the results tend to support the heterogeneous
309 reaction of NO₂ on the surface of BB aerosols were the major contributors to the
310 observed increase of HONO concentration during BB periods.

311 **3.2.3 Roles of BB aerosols in HONO chemistry**

312 The surface area and chemical nature of aerosol particles are the two dominating

313 factors that influence the heterogeneous conversion of NO_2 to produce HONO. In this
314 study, the enhanced aerosol particle loadings associated with the BB plumes (Figs. 1
315 and 3a), providing large aerosol surface areas (Fig. 7a), should aid the conversion of
316 NO_2 to HONO. Beside particle mass concentration, also the particle specific surface
317 area related to the particle size distribution and morphology influences the total
318 particle surface area concentration. In Fig. 7a, we present the relationship between the
319 particle surface area and particle mass concentration ($\text{PM}_{2.5}$) for both the BB and
320 non-BB samples. The slope of the data pairs for BB samples was almost twice as that
321 of non-BB aerosols, suggesting a much higher specific surface area for BB aerosols
322 than that for non-BB aerosols. To further verify this point and find out the causes, we
323 selected the samples with the $\text{PM}_{2.5}$ mass in the overlap concentration range 100–150
324 $\mu\text{g m}^{-3}$ during both BB and non-BB periods (Fig. 7a and 7b), and compared their
325 surface area concentrations calculated by the size distribution (Fig. 7c). The results
326 showed an evidently larger surface area concentration for BB aerosols compared with
327 non-BB aerosols. These results clearly suggest that BB aerosols have a larger specific
328 surface area than non-BB aerosol, which is caused by a much high number of
329 accumulation mode particles, and favor NO_2 to HONO conversion at similar levels of
330 the PM mass concentration. To further investigate the influence of BB aerosols on the
331 particle specific surface area, we plotted the ratios of particle surface area to $\text{PM}_{2.5}$
332 against the abundance of potassium in $\text{PM}_{2.5}$ (Fig. 8) during BB periods. The result
333 showed a positively linear correlation between the two metrics, suggesting a strong
334 enhancement of BB aerosols on the particle specific area concentrations. Besides the
335 surface area concentrations, the chemical nature of aerosols, which control the NO_2
336 conversion efficiency, is also a candidate influencing the transformation of NO_2 to
337 HONO.

338 The NO_2 conversion efficiency refers to the ability of the interface to convert NO_2 to
339 HONO. In the ambient air, both aerosol and ground surface contribute to the
340 HONO/NO_2 ratio. Therefore, the NO_2 conversion efficiency can be represented by
341 $(\text{HONO}/\text{NO}_2) / (\text{particle surface area} + \text{ground surface area})$ when the NO_2 and

342 HONO were balanced to each other (02:00-05:59, see Fig. 6). Here, we assume the
343 related ground surface areas for each BB or non-BB sample are the same. In such case,
344 the ratios of $(\text{HONO}/\text{NO}_2) / (\text{ground surface} + \text{aerosol surface})$ can only be compared
345 when the aerosol surface areas of BB and non-BB aerosols were the same. Therefore,
346 we selected the balanced samples with the surface area concentrations in the
347 overlapped range $1.5\text{--}2.2 \times 10^{-9} \text{ m}^2 \text{ cm}^{-3}$, and compared the ratios of $(\text{HONO}/\text{NO}_2) /$
348 (aerosol surface) to instead the comparison of $(\text{HONO}/\text{NO}_2) / (\text{ground surface} +$
349 $\text{aerosol surface})$. As showed in Fig. 9, the values of this ratio were 67% higher for BB
350 samples than those for non-BB samples, further suggesting the NO_2 conversion
351 efficiency of BB aerosols was higher than that of Non-BB aerosols.

352 In summary, the elevated HONO formation observed in BB plumes was caused by the
353 combined effects of enhanced particle loadings, higher specific aerosol surface areas,
354 and more efficient conversion of NO_2 to HONO on particle surfaces. It is well known
355 that high particle loadings associated with BB are caused by both primary particle
356 emissions and secondary aerosol formation during the atmospheric transport (Andreae
357 and Merlet, 2001; Li et al., 2003; Capes et al., 2008). Large aerosol specific surface
358 areas are probably due to the extremely high number concentrations of accumulation
359 mode particles during BB (Janhäll et al., 2010), and possibly the irregular shape of
360 soot particles (Dobbins and Megaridis, 1987; Cai et al., 1993), which is one major
361 product of BB. The higher NO_2 to HONO conversion efficiency on particle surfaces
362 in BB plumes compared with non-BB air is a complex issue. One possible reason is
363 the high abundance of organic (e.g. humic like) substances and soot particles (Reid et
364 al., 2005), which are high-performance media to convert NO_2 to HONO. This is
365 supported by the much higher concentrations of organics and black carbons, which
366 were estimated as the differences of $\text{PM}_{2.5}$ and the water-soluble ions, in BB periods
367 than those in Non-BB periods (see Fig. 3b).

368 **3.3 Influence of mixed plume of biomass burning and fossil fuel emissions on** 369 **HONO chemistry**

370 An intense BB episode mixed with FF emissions that significantly influenced the
371 everyday weather was observed on 10 June, 2012 (from 18:00 on 9 June to 05:00 on
372 11 June) (Ding et al., 2013b). Interestingly, the highest mixing ratios of HONO,
373 exceeding 5 ppbv, occurred during this episode (Fig. 1). The solar radiation intensity
374 was significantly decreased in the daytime of this episode due to the extremely high
375 particle loading (See Fig. 3 in Ding et al., 2013b), and HONO concentrations during
376 the daytime were at a similar level as those during the nighttime. Again, we
377 investigated the relation between HONO and potassium. The result showed no
378 correlation (slop=-0.08, R=0.24, figure not shown), suggesting that the enhanced
379 HONO concentrations during the case of 10 June were secondarily produced.
380 Although a high particle loading should be a contributor to the high HONO levels, it
381 was not likely the most predominant factor because the PM concentrations during this
382 event were comparable to the peak concentrations during the other BB episodes (Fig.
383 1). Another possible reason is that the plumes on 10 June were more aged than the
384 other BB plumes, which would enhance the HONO production with a longer NO₂
385 contact time with aerosol and ground surface. However, as showed in Fig. 6, HONO
386 and NO₂ can be balanced to each other and reach a steady state in 8 hours. The
387 balanced values of HONO/NO₂ ratios were 0.083 ± 0.014 (the value for 03:00) for
388 other BB plumes, which were still much lower than those in June 10 case ($0.17 \pm$
389 0.046), suggesting some other factors other than the plume age enhanced the HONO
390 concentrations during 10 June.

391 Figure 12 shows the scatter plot between HONO and NO₂ concentrations during the
392 BB periods. The dataset was separated into two groups: the first 5 hours of 10 June
393 (red squares, 18:00-22:00, on 9 June) combined with other BB episodes (blue squares)
394 and later stage of the 10 June case (green circle dots). Both groups revealed a strong
395 relation between HONO and NO₂ with a correlation coefficient higher than 0.8. The
396 slope of the regression of the latter stage of the 10 June case was almost twice as that
397 of the other group (0.12 vs 0.07), indicating a higher NO₂ to HONO conversion
398 potential of the aerosols in the later stage of the 10 June case compared with other BB

399 episodes.

400 To further verify this point and exclude the influence of particle loading, samples with
401 $\text{PM}_{2.5}$ concentrations in range of 190–300 $\mu\text{g m}^{-3}$ (the overlapping parts) were
402 selected from both groups. Although the selected samples had similar PM
403 concentration levels (Fig. 11a), the HONO/ NO_2 ratios (Fig. 11b) and ratios between
404 HONO/ NO_2 and $\text{PM}_{2.5}$ (Fig. 11c) were much higher on 10 June than those during the
405 other BB episodes, indicating a higher potential for the aerosols on 10 June to convert
406 NO_2 to HONO. It should be noted that particle surface area data were not available for
407 the 10 June case because the extremely high particle loading influenced the sample
408 inlet of the DMPS. The exact contributors to the enhancement of NO_2 conversion
409 potentials, which was either higher specific aerosol surface areas or stronger
410 conversion efficiency, are therefore not clear.

411 Our previous study demonstrated that the episode on 10 June was caused by not only
412 BB but a mixture of intense BB and anthropogenic FF emissions (Ding et al., 2013b).
413 As shown in Fig. 12, the SO_2 concentration was low at the beginning of this episode
414 and then gradually increased, suggesting the mixing of anthropogenic pollutions rich
415 in SO_2 with the BB particles several hours after the invasion of the BB plume. This is
416 why the chemical features (HONO/ NO_2) in the plume of the beginning stage of the 10
417 June case was similar to that in other BB episodes, yet very different from the later
418 stage of the 10 June case (Fig. 10).

419 The mix of BB plumes and FF emissions will promote the formation of secondary
420 aerosols (e. g. sulfate and secondary organic aerosols (SOA)) on BB particles, and
421 thus modify their morphology and surface chemical nature (Li et al., 2003; Capes et
422 al., 2008). As shown in Fig. 12d, the abundance of sulfate in $\text{PM}_{2.5}$ was significantly
423 enhanced in 10 June case compared with other BB episodes. This coincided with the
424 high NO_2 to HONO conversion efficiency (Fig. 12c), indicating a promotion of
425 secondary aerosol formation on BB particles in the mixed plumes to produce HONO.
426 To further verify this point, we plotted the nighttime HONO concentration against the

427 sulfate concentration on 10 June (Fig. 13), noting that the daytime HONO chemistry
428 is out of the scope of this work. The result shows a very good correlation between the
429 two compounds ($R=0.79$), further suggesting the promotion of secondary aerosol
430 formation on BB particles to HONO formation.

431 As discussed above, the specific surface area and chemical nature of aerosol particles
432 are the key factors in determining their potential to convert NO_2 to HONO. Therefore,
433 changes in the morphology and size distribution caused by secondary aerosol
434 formation may have enhanced the specific surface area and led to increased HONO
435 production in the mixed plumes. Besides, the enhanced aerosol water content (Fig. 12)
436 caused by the production of hydrophilic species, e.g. sulfate, may also play a role in
437 accelerating the NO_2 conversion (Stutz et al., 2004). Another factor that might have
438 enhanced HONO production could be the formation of some specific secondary
439 material on BB particles, e.g. sulfate (Kleffmann et al., 1998) and secondary organic
440 aerosols (Bröske et al., 2003).

441 **4. Conclusions and implications**

442 In this study, we analyzed a two-month measurement of atmospheric HONO during
443 the BB season of 2012 (May and June) at the SORPES station in western YRD of
444 eastern China, and demonstrated an important role of BB in the HONO chemistry in
445 the ambient atmosphere. Direct emissions from BB have been estimated to contribute
446 $17\% \pm 12\%$ of the observed HONO concentrations during nighttime BB episodes. The
447 other over 80% was produced by the heterogeneous conversion of NO_2 . The
448 NO_2 -to-HONO (C_{HONO}) conversion rates were detected to be significantly elevated
449 during the BB periods due to the combined effect of enhanced particle loadings, larger
450 specific surface areas of particles and higher NO_2 conversion efficiency on BB
451 aerosols. An episode of mixed plumes of intense BB and anthropogenic FF emissions
452 was observed on 10 June, during which the HONO production potentials from the
453 conversion of NO_2 was further promoted by the formation of secondary particulate
454 matters on BB particles.

455 Given that BB plumes are easily mixed with other anthropogenic pollutants in eastern
456 China, their influences on the atmospheric chemistry is expected to be important via
457 affecting the HONO budget and thus the radical pool. Furthermore, considering the
458 potential re-activation of BB particles (e.g. soot) during their atmospheric transport,
459 the HONO chemistry associated with BB plumes may affect atmospheric chemistry
460 long distances downwind BB areas, even in the marine boundary layer. Therefore,
461 more studies are encouraged on BB related chemistry in eastern China, which is a
462 unique “laboratory” with frequent mixed plumes of BB and anthropogenic pollutions.

463 **Acknowledgements**

464 This work was funded by National Natural Science Foundation of China
465 (D0512/0207131138 and D0510/41275129), the MOST 973 Program
466 (2010CB428500), and the Jiangsu Provincial Science Fund for Distinguished Young
467 Scholars (No. BK20140021). We thank T. Wang and L. Xue at The Hong Kong
468 Polytechnic University for their suggestion on the data analysis. We are grateful of
469 J. Kleffmann at Bergische Universität Wuppertal for his useful discussions on the
470 data quality. We thank Metrohm Co. China for providing the MARGA analyzer and Z.
471 Yan and J. Gao for their technical support for the instrument. We also thank the two
472 anonymous referees for their construction and detailed comments during the open
473 discussion of this manuscript (acpd-14-7859-2014).

474

475 **References**

- 476 Acker, K., and Möller, D.: Atmospheric variation of nitrous acid at different sites in Europe,
477 Environ. Chem., 4, 242-255, 10.1071/EN07023, 2007.
- 478 Alicke, B., Platt, U., and Stutz, J.: Impact of nitrous acid photolysis on the total hydroxyl
479 radical budget during the Limitation of Oxidant Production/Pianura Padana Produzione
480 di Ozono study in Milan, J. Geophys. Res.-Atmos., 107, 8196, 10.1029/2000JD000075,
481 2002.
- 482 Ammann, M., Kalberer, M., Jost, D. T., Tobler, L., Rössler, E., Piguet, D., Gägeler, H. W.,
483 and Baltensperger, U.: Heterogeneous production of nitrous acid on soot in polluted air
484 masses, Nature, 395, 157-160, 1998.
- 485 Ammann, M., Rössler, E., Strekowski, R., and George, C.: Nitrogen dioxide multiphase
486 chemistry: Uptake kinetics on aqueous solutions containing phenolic compounds, Phys.
487 Chem. Chem. Phys., 7, 2513-2518, 2005.
- 488 ANDREAE, M. O.: Soot Carbon and Excess Fine Potassium: Long-Range Transport of
489 Combustion-Derived Aerosols, Science, 220, 1148-1151,
490 10.1126/science.220.4602.1148, 1983.
- 491 Andreae, M. O., and Merlet, P.: Emission of trace gases and aerosols from biomass burning,
492 Global Biogeochem. Cy., 15, 955-966, 10.1029/2000gb001382, 2001.
- 493 Appel, B. R., Winer, A. M., Tokiwa, Y., and Biermann, H. W.: Comparison of atmospheric
494 nitrous acid measurements by annular denuder and differential optical absorption
495 systems, Atmos. Environ. Part A. General Topics, 24, 611-616,
496 10.1016/0960-1686(90)90016-G, 1990.
- 497 Aubin, D. G., and Abbatt, J. P. D.: Interaction of NO₂ with Hydrocarbon Soot: Focus on
498 HONO Yield, Surface Modification, and Mechanism, J. Phys. Chem. A, 111, 6263-6273,
499 10.1021/jp068884h, 2007.
- 500 Aumont, B., Madronich, S., Ammann, M., Kalberer, M., Baltensperger, U., Hauglustaine, D.,
501 and Brocheton, F.: On the NO₂ + soot reaction in the atmosphere, J. Geophys.
502 Res.-Atmos., 104, 1729-1736, 10.1029/1998jd100023, 1999.

503 Barnes, I., and Rudziński, K. J.: Disposal of Dangerous Chemicals in Urban Areas and Mega
504 Cities-Role of Oxides and Acids of Nitrogen in Atmospheric Chemistry, Springer, 2012.

505 Bedjanian, Y., and El Zein, A.: Interaction of NO₂ with TiO₂ Surface Under UV Irradiation:
506 Products Study, *J. Phys. Chem. A*, 116, 1758-1764, 10.1021/jp210078b, 2012.

507 Bröske, R., Kleffmann, J., and Wiesen, P.: Heterogeneous conversion of NO₂ on secondary
508 organic aerosol surfaces: A possible source of nitrous acid (HONO) in the atmosphere?,
509 *Atmos. Chem. Phys.*, 3, 469-474, 10.5194/acp-3-469-2003, 2003.

510 Burling, I. R., Yokelson, R. J., Griffith, D. W. T., Johnson, T. J., Veres, P., Roberts, J. M.,
511 Warneke, C., Urbanski, S. P., Reardon, J., Weise, D. R., Hao, W. M., and de Gouw, J.:
512 Laboratory measurements of trace gas emissions from biomass burning of fuel types
513 from the southeastern and southwestern United States, *Atmos. Chem. Phys.*, 10,
514 11115-11130, 10.5194/acp-10-11115-2010, 2010.

515 Cai, J., Lu, N., and Sorensen, C. M.: Comparison of size and morphology of soot aggregates
516 as determined by light scattering and electron microscope analysis, *Langmuir*, 9,
517 2861-2867, 10.1021/la00035a023, 1993.

518 Capes, G., Johnson, B., McFiggans, G., Williams, P. I., Haywood, J., and Coe, H.: Aging of
519 biomass burning aerosols over West Africa: Aircraft measurements of chemical
520 composition, microphysical properties, and emission ratios, *J. Geophys. Res.-Atmos.*,
521 113, D00C15, 10.1029/2008JD009845, 2008.

522 Ding, A., Wang, T., and Fu, C.: Transport characteristics and origins of carbon monoxide and
523 ozone in Hong Kong, South China, *J. Geophys. Res.-Atmos.*, 118, 9475-9488,
524 10.1002/jgrd.50714, 2013a.

525 Ding, A. J., Fu, C. B., Yang, X. Q., Sun, J. N., Petäjä T., Kerminen, V. M., Wang, T., Xie, Y.,
526 Herrmann, E., Zheng, L. F., Nie, W., Liu, Q., Wei, X. L., and Kulmala, M.: Intense
527 atmospheric pollution modifies weather: a case of mixed biomass burning with fossil
528 fuel combustion pollution in eastern China, *Atmos. Chem. Phys.*, 13, 10545-10554,
529 10.5194/acp-13-10545-2013, 2013b.

530 Ding, A. J., Fu, C. B., Yang, X. Q., Sun, J. N., Zheng, L. F., Xie, Y. N., Herrmann, E., Nie,

531 W., Petäjä T., Kerminen, V. M., and Kulmala, M.: Ozone and fine particle in the
532 western Yangtze River Delta: an overview of 1 yr data at the SORPES station, *Atmos.*
533 *Chem. Phys.*, 13, 5813-5830, 10.5194/acp-13-5813-2013, 2013c.

534 Dobbins, R. A., and Megaridis, C. M.: Morphology of flame-generated soot as determined by
535 thermophoretic sampling, *Langmuir*, 3, 254-259, 1987.

536 Donaldson, M. A., Berke, A. E., and Raff, J. D.: Uptake of Gas Phase Nitrous Acid onto
537 Boundary Layer Soil Surfaces, *Environ. Sci. Technol.*, 48, 375-383, 10.1021/es404156a,
538 2013.

539 Elshorbany, Y., Barnes, I., Becker, K. H., Kleffmann, J., and Wiesen, P.: Sources and cycling
540 of tropospheric hydroxyl radicals—an overview, *Int. J. Res. Phys. Chem. Chem. Phys.*,
541 2010.

542 Elshorbany, Y. F., Steil, B., Brühl, C., and Lelieveld, J.: Impact of HONO on global
543 atmospheric chemistry calculated with an empirical parameterization in the EMAC
544 model, *Atmos. Chem. Phys.*, 12, 9977-10000, 10.5194/acp-12-9977-2012, 2012.

545 Elshorbany, Y. F., Crutzen, P. J., Steil, B., Pozzer, A., Tost, H., and Lelieveld, J.: Global and
546 regional impacts of HONO on the chemical composition of clouds and aerosols, *Atmos.*
547 *Chem. Phys.*, 14, 1167-1184, 10.5194/acp-14-1167-2014, 2014.

548 Genfa, Z., Slanina, S., Brad Boring, C., Jongejan, P. A. C., and Dasgupta, P. K.: Continuous
549 wet denuder measurements of atmospheric nitric and nitrous acids during the 1999
550 Atlanta Supersite, *Atmos. Environ.*, 37, 1351-1364, 10.1016/S1352-2310(02)01011-7,
551 2003.

552 George, C., Strekowski, R. S., Kleffmann, J., Stemmler, K., and Ammann, M.:
553 Photoenhanced uptake of gaseous NO₂ on solid organic compounds: a photochemical
554 source of HONO?, *Faraday Discuss.*, 130, 195-210, 10.1039/b417888m, 2005.

555 Gonçalves, M., Dabdub, D., Chang, W. L., Jorba, O., and Baldasano, J. M.: Impact of HONO
556 sources on the performance of mesoscale air quality models, *Atmos. Environ.*, 54,
557 168-176, 10.1016/j.atmosenv.2012.02.079, 2012.

558 Harrison, R. M., and Collins, G. M.: Measurements of Reaction Coefficients of NO₂ and

559 HONO on Aerosol Particles, *J. Atmos. Chem.*, 30, 397-406, 10.1023/a:1006094304069,
560 1998.

561 Harrison, R. M., and Kitto, A.-M. N.: Evidence for a surface source of atmospheric nitrous
562 acid, *Atmos. Environ.*, 28, 1089-1094, 10.1016/1352-2310(94)90286-0, 1994.

563 Hofzumahaus, A., Rohrer, F., Lu, K., Bohn, B., Brauers, T., Chang, C.-C., Fuchs, H., Holland,
564 F., Kita, K., Kondo, Y., Li, X., Lou, S., Shao, M., Zeng, L., Wahner, A., and Zhang, Y.:
565 Amplified Trace Gas Removal in the Troposphere, *Science*, 324, 1702-1704,
566 10.1126/science.1164566, 2009.

567 Janháňal, S., Andreae, M. O., and Pöschl, U.: Biomass burning aerosol emissions from
568 vegetation fires: particle number and mass emission factors and size distributions, *Atmos.*
569 *Chem. Phys.*, 10, 1427-1439, 10.5194/acp-10-1427-2010, 2010.

570 Kalberer, M., Ammann, M., Arens, F., Gäggeler, H. W., and Baltensperger, U.:
571 Heterogeneous formation of nitrous acid (HONO) on soot aerosol particles, *J. Geophys.*
572 *Res.-Atmos.*, 104, 13825-13832, 10.1029/1999jd900141, 1999.

573 Kleffmann, J., Becker, K. H., and Wiesen, P.: Heterogeneous NO₂ conversion processes on
574 acid surfaces: possible atmospheric implications, *Atmos. Environ.*, 32, 2721-2729,
575 10.1016/S1352-2310(98)00065-X, 1998.

576 Kleffmann, J., Becker, K. H., Lackhoff, M., and Wiesen, P.: Heterogeneous conversion of
577 NO₂ on carbonaceous surfaces, *Phys. Chem. Chem. Phys.*, 1, 5443-5450,
578 10.1039/a905545b, 1999.

579 Kleffmann, J., Heland, J., Kurtenbach, R., Lorzer, J., and Wiesen, P.: A new instrument
580 (LOPAP) for the detection of nitrous acid (HONO), *Environ. Sci. Pollut. R.*, 48-54,
581 2002.

582 Kleffmann, J., Gavriloaiei, T., Hofzumahaus, A., Holland, F., Koppmann, R., Rupp, L.,
583 Schlosser, E., Siese, M., and Wahner, A.: Daytime formation of nitrous acid: A major
584 source of OH radicals in a forest, *Geophys. Res. Lett.*, 32, L05818,
585 10.1029/2005GL022524, 2005.

586 Kleffmann, J., and Wiesen, P.: Heterogeneous conversion of NO₂ and NO on HNO₃ treated

587 soot surfaces: atmospheric implications, *Atmos. Chem. Phys.*, 5, 77-83,
588 10.5194/acp-5-77-2005, 2005.

589 Kleffmann, J.: Daytime Sources of Nitrous Acid (HONO) in the Atmospheric Boundary
590 Layer, *ChemPhysChem*, 8, 1137-1144, 10.1002/cphc.200700016, 2007.

591 Kurtenbach, R., Becker, K. H., Gomes, J. A. G., Kleffmann, J., Lörzer, J. C., Spittler, M.,
592 Wiesen, P., Ackermann, R., Geyer, A., and Platt, U.: Investigations of emissions and
593 heterogeneous formation of HONO in a road traffic tunnel, *Atmos. Environ.*, 35,
594 3385-3394, 10.1016/S1352-2310(01)00138-8, 2001.

595 Langridge, J. M., Gustafsson, R. J., Griffiths, P. T., Cox, R. A., Lambert, R. M., and Jones, R.
596 L.: Solar driven nitrous acid formation on building material surfaces containing titanium
597 dioxide: A concern for air quality in urban areas?, *Atmos. Environ.*, 43, 5128-5131,
598 10.1016/j.atmosenv.2009.06.046, 2009.

599 Li, G., Lei, W., Zavala, M., Volkamer, R., Dusanter, S., Stevens, P., and Molina, L. T.:
600 Impacts of HONO sources on the photochemistry in Mexico City during the
601 MCMA-2006/MILAGO Campaign, *Atmos. Chem. Phys.*, 10, 6551-6567,
602 10.5194/acp-10-6551-2010, 2010.

603 Li, J., Pósfai, M., Hobbs, P. V., and Buseck, P. R.: Individual aerosol particles from biomass
604 burning in southern Africa: 2, Compositions and aging of inorganic particles, *J. Geophys.*
605 *Res.-Atmos.*, 108, 8484, 10.1029/2002JD002310, 2003.

606 Li, X., Wang, S., Duan, L., Hao, J., Li, C., Chen, Y., and Yang, L.: Particulate and Trace Gas
607 Emissions from Open Burning of Wheat Straw and Corn Stover in China, *Environ. Sci.*
608 *Technol.*, 41, 6052-6058, 10.1021/es0705137, 2007.

609 Li, X., Brauers, T., Häßeler, R., Bohn, B., Fuchs, H., Hofzumahaus, A., Holland, F., Lou, S.,
610 Lu, K. D., Rohrer, F., Hu, M., Zeng, L. M., Zhang, Y. H., Garland, R. M., Su, H., Nowak,
611 A., Wiedensohler, A., Takegawa, N., Shao, M., and Wahner, A.: Exploring the
612 atmospheric chemistry of nitrous acid (HONO) at a rural site in Southern China, *Atmos.*
613 *Chem. Phys.*, 12, 1497-1513, 10.5194/acp-12-1497-2012, 2012.

614 Longfellow, C. A., Ravishankara, A. R., and Hanson, D. R.: Reactive uptake on hydrocarbon

615 soot: Focus on NO₂, *J. Geophys. Res.-Atmos.*, 104, 13833-13840,
616 10.1029/1999jd900145, 1999.

617 Ma, Y., Weber, R. J., Lee, Y. -N., Orsini, D. A., Maxwell-Meier, K., Thornton, D. C., Bandy,
618 A. R., Clarke, A. D., Blake, D. R., Sachse, G. W., Fuelberg, H. E., Kiley, C. M., Woo, J.
619 -H., Streets, D. G., and Carmichael, G. R.: Characteristics and influence of biosmoke on
620 the fine-particle ionic composition measured in Asian outflow during the Transport and
621 Chemical Evolution Over the Pacific (TRACE-P) experiment, *J. Geophys. Res.-Atmos.*,
622 108, 8816, 10.1029/2002JD003128, 2003.

623 Makkonen, U., Virkkula, A., Mäntykerntt ä J., Hakola, H., Keronen, P., Vakkari, V., and Aalto,
624 P. P.: Semi-continuous gas and inorganic aerosol measurements at a Finnish urban site:
625 comparisons with filters, nitrogen in aerosol and gas phases, and aerosol acidity, *Atmos.*
626 *Chem. Phys.*, 12, 5617-5631, 10.5194/acp-12-5617-2012, 2012.

627 Monge, M. E., D'Anna, B., Mazri, L., Giroir-Fendler, A., Ammann, M., Donaldson, D. J.,
628 and George, C.: Light changes the atmospheric reactivity of soot, *P. Natl. Acad. Sci.*
629 *USA*, 107, 6605-6609, 10.1073/pnas.0908341107, 2010.

630 Ndour, M., D'Anna, B., George, C., Ka, O., Balkanski, Y., Kleffmann, J., Stemmler, K., and
631 Ammann, M.: Photoenhanced uptake of NO₂ on mineral dust: Laboratory experiments
632 and model simulations, *Geophys. Res. Lett.*, 35, L05812, 10.1029/2007gl032006, 2008.

633 Nie, W., Wang, T., Xue, L. K., Ding, A. J., Wang, X. F., Gao, X. M., Xu, Z., Yu, Y. C., Yuan,
634 C., Zhou, Z. S., Gao, R., Liu, X. H., Wang, Y., Fan, S. J., Poon, S., Zhang, Q. Z., and
635 Wang, W. X.: Asian dust storm observed at a rural mountain site in southern China:
636 chemical evolution and heterogeneous photochemistry, *Atmos. Chem. Phys.*, 12,
637 11985-11995, 10.5194/acp-12-11985-2012, 2012.

638 Platt, U., Perner, D., Harris, G. W., Winer, A. M., and Pitts, J. N.: Observations of nitrous
639 acid in an urban atmosphere by differential optical absorption, *Nature*, 285, 312- 314,
640 doi:10.1038/285312a0, 1980.

641 Prince, A. P., Wade, J. L., Grassian, V. H., Kleiber, P. D., and Young, M. A.: Heterogeneous
642 reactions of soot aerosols with nitrogen dioxide and nitric acid: atmospheric chamber
643 and Knudsen cell studies, *Atmos. Environ.*, 36, 5729-5740,

644 10.1016/S1352-2310(02)00626-X, 2002.

645 Reid, J. S., Koppmann, R., Eck, T. F., and Eleuterio, D. P.: A review of biomass burning
646 emissions part II: intensive physical properties of biomass burning particles, *Atmos.*
647 *Chem. Phys.*, 5, 799-825, 10.5194/acp-5-799-2005, 2005.

648 Roberts, J. M., Veres, P., Warneke, C., Neuman, J. A., Washenfelder, R. A., Brown, S. S.,
649 Baasandorj, M., Burkholder, J. B., Burling, I. R., Johnson, T. J., Yokelson, R. J., and de
650 Gouw, J.: Measurement of HONO, HNCO, and other inorganic acids by negative-ion
651 proton-transfer chemical-ionization mass spectrometry (NI-PT-CIMS): application to
652 biomass burning emissions, *Atmos. Meas. Tech.*, 3, 981-990, 10.5194/amt-3-981-2010,
653 2010.

654 Sörgel, M., Regelin, E., Bozem, H., Diesch, J. M., Drewnick, F., Fischer, H., Harder, H., Held,
655 A., Hosaynali-Beygi, Z., Martinez, M., and Zetzsch, C.: Quantification of the unknown
656 HONO daytime source and its relation to NO₂, *Atmos. Chem. Phys.*, 11, 10433-10447,
657 10.5194/acp-11-10433-2011, 2011.

658 Sander, S. P., Golden, D., Kurylo, M., Moortgat, G., Wine, P., Ravishankara, A., Kolb, C.,
659 Molina, M., Finlayson-Pitts, B., and Huie, R.: Chemical kinetics and photochemical data
660 for use in atmospheric studies evaluation number 15, 2006.

661 Simoneit, B. R. T.: Biomass burning — a review of organic tracers for smoke from
662 incomplete combustion, *Appl. Geochem.*, 17, 129-162, 10.1016/S0883-2927(01)00061-0,
663 2002.

664 Spindler, G., Hesper, J., Brüggemann, E., Dubois, R., Müller, Th., and Herrmann, H.: Wet
665 annular denuder measurements of nitrous acid: laboratory study of the artefact reaction
666 of NO₂ with S(IV) in aqueous solution and comparison with field measurements, *Atmos.*
667 *Environ.*, 37, 2643-2662, 10.1016/S1352-2310(03)00209-7, 2003.

668 Stemmler, K., Ammann, M., Donders, C., Kleffmann, J., and George, C.: Photosensitized
669 reduction of nitrogen dioxide on humic acid as a source of nitrous acid, *Nature*, 440,
670 195-198, 2006.

671 Stockwell, C. E., Yokelson, R. J., Kreidenweis, S. M., Robinson, A. L., DeMott, P. J.,

672 Sullivan, R. C., Reardon, J., Ryan, K. C., Griffith, D. W. T., and Stevens, L.: Trace gas
673 emissions from combustion of peat, crop residue, domestic biofuels, grasses, and other
674 fuels: configuration and Fourier transform infrared (FTIR) component of the fourth Fire
675 Lab at Missoula Experiment (FLAME-4), *Atmos. Chem. Phys.*, 14, 9727-9754,
676 10.5194/acp-14-9727-2014, 2014.

677 Stutz, J., Alicke, B., and Neftel, A.: Nitrous acid formation in the urban atmosphere: Gradient
678 measurements of NO₂ and HONO over grass in Milan, Italy, *J. Geophys. Res.-Atmos.*,
679 107, 2002.

680 Stutz, J., Alicke, B., Ackermann, R., Geyer, A., Wang, S., White, A. B., Williams, E. J.,
681 Spicer, C. W., and Fast, J. D.: Relative humidity dependence of HONO chemistry in
682 urban areas, *J. Geophys. Res.-Atmos.*, 109, D03307, 10.1029/2003JD004135, 2004.

683 Su, H.: HONO: a Study to its Sources and Impacts from Field Measurements at the Sub-urban
684 Areas of PRD Region, PhD Thesis of Peking University, 2008.

685 Su, H., Cheng, Y. F., Shao, M., Gao, D. F., Yu, Z. Y., Zeng, L. M., Slanina, J., Zhang, Y. H.,
686 and Wiedensohler, A.: Nitrous acid (HONO) and its daytime sources at a rural site
687 during the 2004 PRIDE-PRD experiment in China, *J. Geophys. Res.-Atmos.*, 113,
688 D14312, 10.1029/2007jd009060, 2008.

689 Su, H., Cheng, Y., Oswald, R., Behrendt, T., Trebs, I., Meixner, F. X., Andreae, M. O., Cheng,
690 P., Zhang, Y., and Pöschl, U.: Soil Nitrite as a Source of Atmospheric HONO and OH
691 Radicals, *Science*, 333, 1616-1618, 10.1126/science.1207687, 2011.

692 Muller, Th., Dubois, R., Spindler, G., Brüggemann, E., Ackermann, R., Geyer, A., and Platf,
693 U.: Measurements of Nitrous Acid by DOAS and Diffusion Denuders: A Comparison,
694 *Transactions on Ecology and the Environment*, 28, ISSN 1743-3541, 1999.

695 VandenBoer, T. C., Brown, S. S., Murphy, J. G., Keene, W. C., Young, C. J., Pszenny, A. A.
696 P., Kim, S., Warneke, C., de Gouw, J. A., Maben, J. R., Wagner, N. L., Riedel, T. P.,
697 Thornton, J. A., Wolfe, D. E., Dubé W. P., Öztürk, F., Brock, C. A., Grossberg, N.,
698 Lefer, B., Lerner, B., Middlebrook, A. M., and Roberts, J. M.: Understanding the role of
699 the ground surface in HONO vertical structure: High resolution vertical profiles during
700 NACHTT-11, *J. Geophys. Res.-Atmos.*, 118, 10,155-110,171, 10.1002/jgrd.50721,

701 2013.

702 Veres, P., Roberts, J. M., Burling, I. R., Warneke, C., de Gouw, J., and Yokelson, R. J.:
703 Measurements of gas-phase inorganic and organic acids from biomass fires by
704 negative-ion proton-transfer chemical-ionization mass spectrometry, *J. Geophys.*
705 *Res.-Atmos.*, 115, D23302, 10.1029/2010jd014033, 2010.

706 Wang, S., Zhou, R., Zhao, H., Wang, Z., Chen, L., and Zhou, B.: Long-term observation of
707 atmospheric nitrous acid (HONO) and its implication to local NO₂ levels in Shanghai,
708 China, *Atmos. Environ.*, 77, 718-724, 10.1016/j.atmosenv.2013.05.071, 2013.

709 Wang, T., Wong, C. H., Cheung, T. F., Blake, D. R., Arimoto, R., Baumann, K., Tang, J.,
710 Ding, G. A., Yu, X. M., Li, Y. S., Streets, D. G., and Simpson, I. J.: Relationships of
711 trace gases and aerosols and the emission characteristics at Lin'an, a rural site in eastern
712 China, during spring 2001, *J. Geophys. Res.-Atmos.*, 109, D19S05,
713 10.1029/2003JD004119, 2004.

714 Xu, Z., Wang, T., Xue, L. K., Louie, P. K. K., Luk, C. W. Y., Gao, J., Wang, S. L., Chai, F.
715 H., and Wang, W. X.: Evaluating the uncertainties of thermal catalytic conversion in
716 measuring atmospheric nitrogen dioxide at four differently polluted sites in China,
717 *Atmos. Environ.*, 76, 221-226, 10.1016/j.atmosenv.2012.09.043, 2013.

Figure Captions:

Fig. 1 Temporal variation of the concentrations of HONO, NO₂, PM_{2.5} mass and potassium, at the SORPES station during late April to June 2012. Biomass burning episodes were mostly occurred during late May and early June (shaded in the figure).

Fig. 2 Whisker plot of diurnal variation of (a) HONO and (b) HONO/NO₂ at the SORPES station during April to June 2012.

Fig. 3 Comparisons between biomass burning periods (203 samples) and non-biomass burning period (1122 samples) of (a) PM_{2.5} concentrations, (b) concentrations of organic matters in PM_{2.5} (estimated by PM_{2.5}-WSIs), (c) NO₂ concentrations, (d) HONO concentrations, (e) HONO to NO₂ ratio and (f) HONO to NO_x ratio. There are statistically significant differences for all the data pairs ($p \ll 0.01$) except NO₂ ($p = 0.51$).

Fig. 4 Map of 8-hr Lagrangian backward retroplume (100 m footprint layer) for (a) biomass burning air masses (defined as $K^+ > 2 \text{ ug m}^{-3}$ and $K^+/PM > 2\%$) during night time, and (b) non-biomass burning air masses (defined as $K^+ < 2 \text{ ug m}^{-3}$ and $K^+/PM < 2\%$) and active fire (pink dots) during 1 June - 15 June, 2012 (Data obtained from FIRMS MODIS Fire Archive).

Fig. 5 Scatter plot between the HONO and potassium concentration during biomass burning periods

Fig. 6 Ratios of HONO to NO₂ for nighttime samples of BB (except of the June 10 case) and Non-BB plumes. The change rates were calculated from 19:00 to 03:00. Error bars are the standard deviations.

Fig. 7 (a) Scatter plot between the particle surface area and PM_{2.5} for nighttime samples during BB and Non-BB periods, (b) Whisker plot of PM_{2.5} in the selected mass concentration range ($100\text{--}150 \mu\text{g m}^{-3}$, showed in Fig. 7a) during BB (51 samples) and Non-BB period (27 samples), and (c) particle surface area size distributions for the same subsets of data

Fig. 8 Scatter plot between the ratio of particle surface area to $PM_{2.5}$ and the abundance of potassium in $PM_{2.5}$ for nighttime samples during BB during BB period.

Fig. 9 Whisker plot of the ratios between HONO/ NO_2 and particle surface area concentration in the selected particle surface area range ($1.5-2.2 \times 10^{-9} \text{ m}^2 \text{ cm}^{-3}$) during the BB (14 samples) and non-BB periods (21 samples).

Fig. 10 Scatter plot between HONO and NO_2 concentration during the BB periods (without the case of 10th June, blue solid squares), the beginning (red solid diamonds) and latter (green dots) state of the June 10th episode.

Fig. 11 Whisker plots of (a) $PM_{2.5}$ mass, (b) ratios of HONO to NO_2 , (c) ratios of HONO/ NO_2 to $PM_{2.5}$ mass, (d) ratios of sulfate to $PM_{2.5}$, in the selected $PM_{2.5}$ mass concentration range ($190 - 300 \mu\text{g m}^{-3}$) in BB plume (10 samples) and the mixed plume (27 samples).

Fig. 12 Temporal variations of HONO, HONO/ NO_2 ratios, RH, $PM_{2.5}$, sulfate in $PM_{2.5}$ and SO_2 during 9 - 11 June 2012 at the SORPES station

Fig. 13 Scatter plot between HONO and sulfate concentration in $PM_{2.5}$ during the nighttime on 10 June.

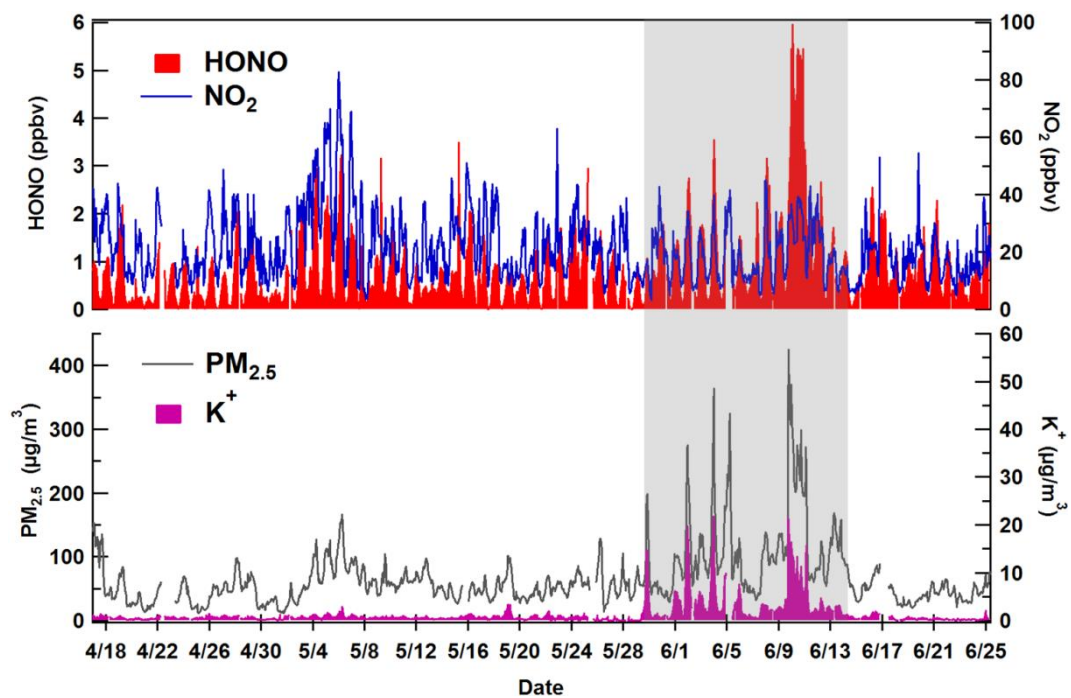


Fig. 1 Temporal variation of the concentrations of HONO, NO₂, PM_{2.5} mass and potassium, at the SORPES central site during late April to June 2012. Biomass burning episodes were mostly occurred during late May and early June (shaded in the figure).

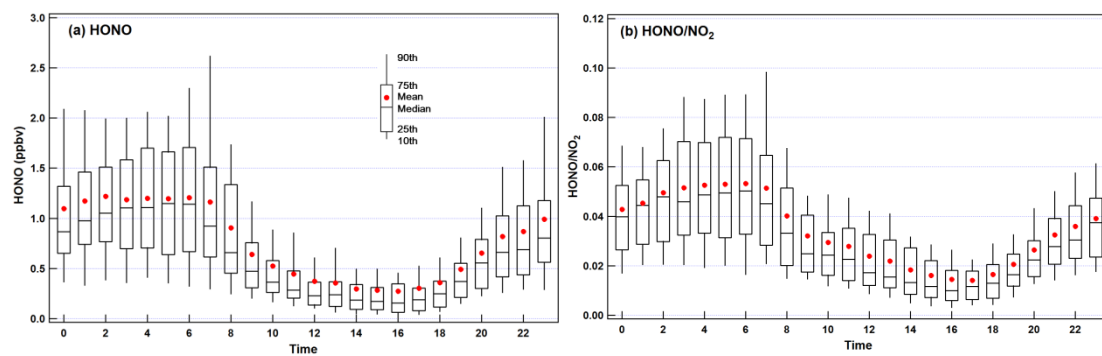


Fig. 2 Whisker plot of diurnal variation of (a) HONO and (b) HONO/NO₂ at the SORPES station during April to June 2012.

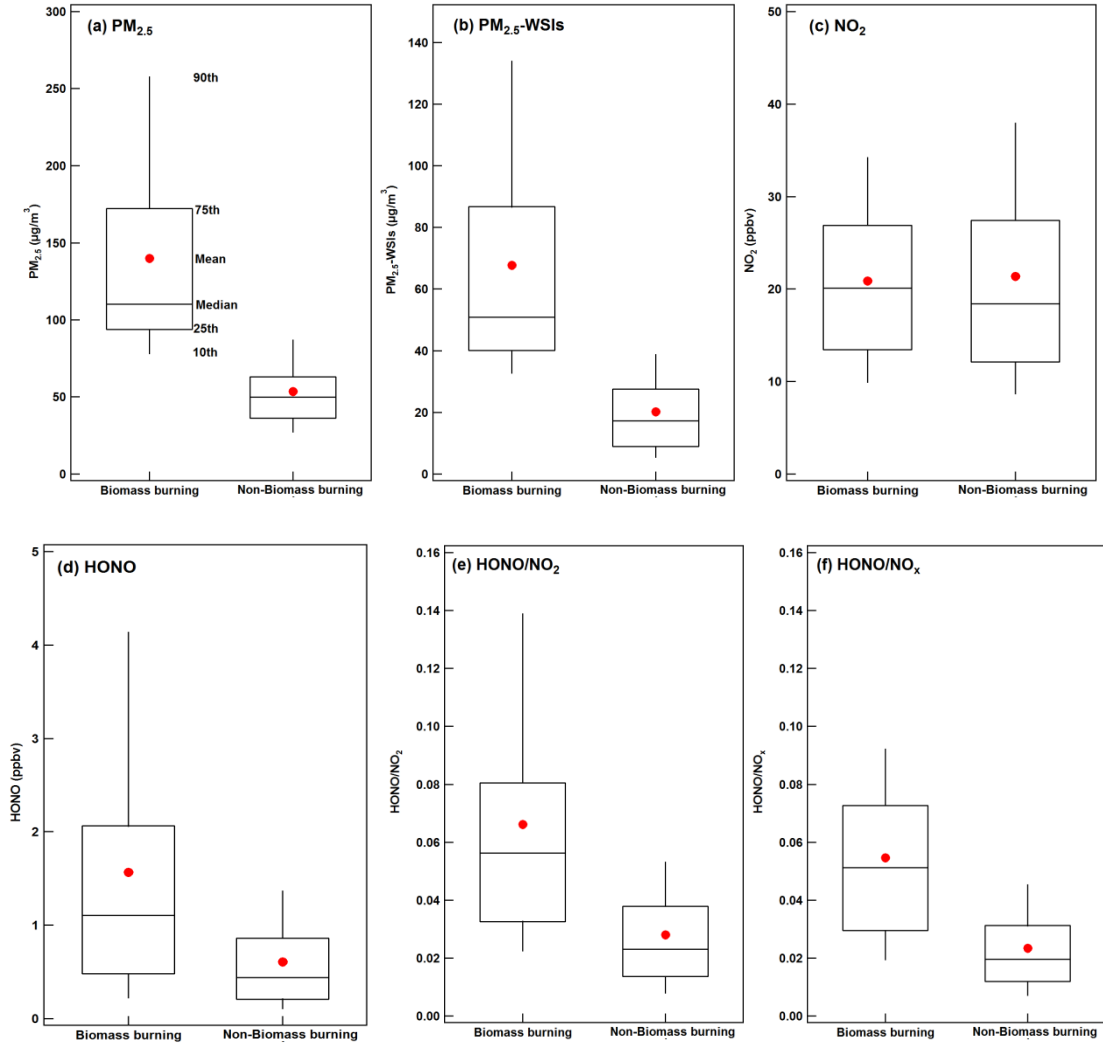


Fig. 3 Comparisons between biomass burning periods (1122 samples) and non-biomass burning period (203 samples) of (a) PM_{2.5} concentrations, (b) concentrations of organic matters in PM_{2.5} (estimated by PM_{2.5}-WSIs), (c) NO₂ concentrations, (d) HONO concentrations, (e) HONO to NO₂ ratio and (f) HONO to NO_x ratio. There are statistically significant differences for all the data pairs ($p < 0.01$) except NO₂ ($p = 0.51$).

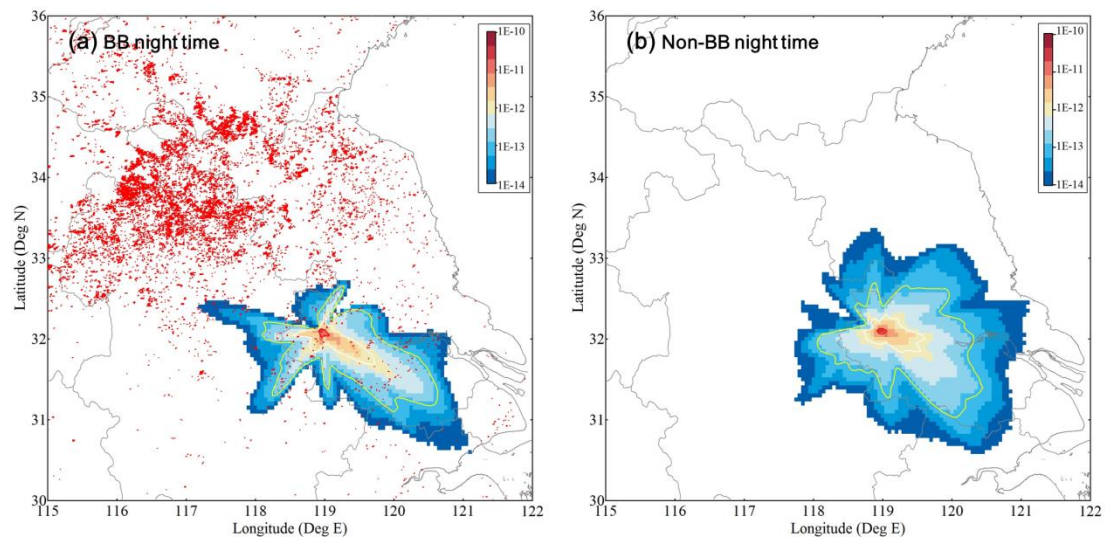


Fig. 4 Map of 8-hr Lagrangian backward retroplume (100 m footprint layer) for (a) biomass burning air masses (defined as $K^+ > 2 \text{ ug m}^{-3}$ and $K^+/PM > 2\%$) during night time, and (b) non-biomass burning air masses (defined as $K^+ < 2 \text{ ug m}^{-3}$ and $K^+/PM < 2\%$) and active fire (pink dots) during 1 June - 15 June, 2012 (Data obtained from FIRMS MODIS Fire Archive).

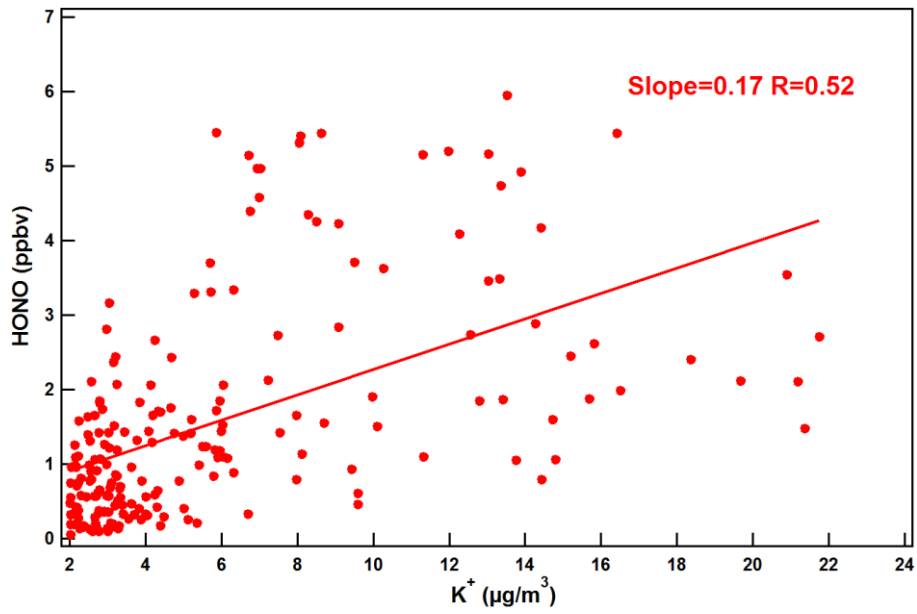


Fig. 5 Scatter plot between the HONO and potassium concentration during biomass burning periods.

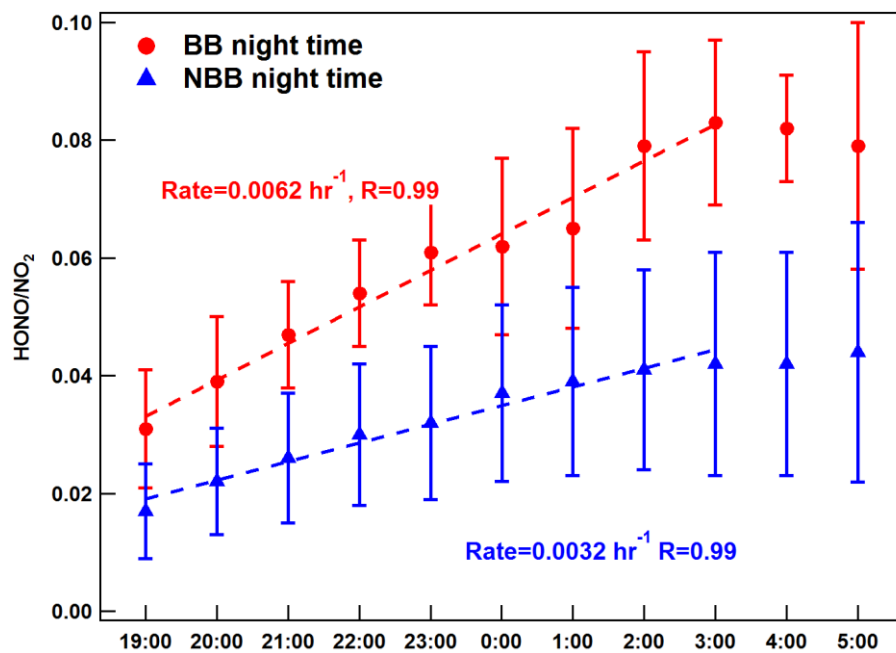


Fig. 6 Ratios of HONO to NO₂ for nighttime samples of BB (except of the June 10 case) and Non-BB plumes. The change rates were calculated from 19:00 to 03:00. Error bars are the standard deviations.

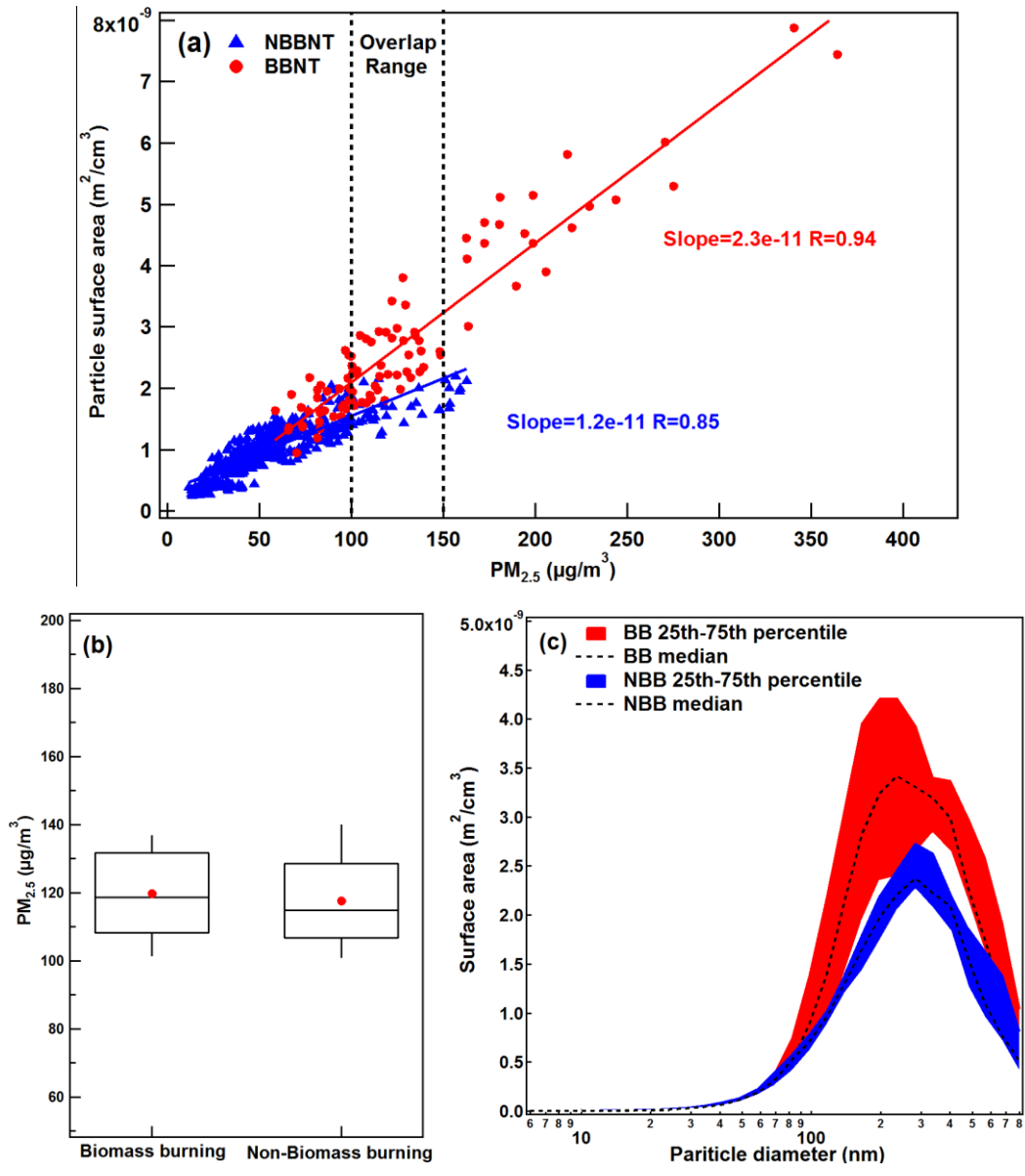


Fig. 7 (a) Scatter plot between the particle surface area and $\text{PM}_{2.5}$ for nighttime samples of BB and Non-BB plumes, (b) Whisker plot of $\text{PM}_{2.5}$ in the selected mass concentration range ($100\text{--}150\mu\text{g m}^{-3}$, showed in Fig. 7a) during BB (51 samples) and Non-BB period (27 samples), and (c) particle surface area size distributions for the same subsets of data.

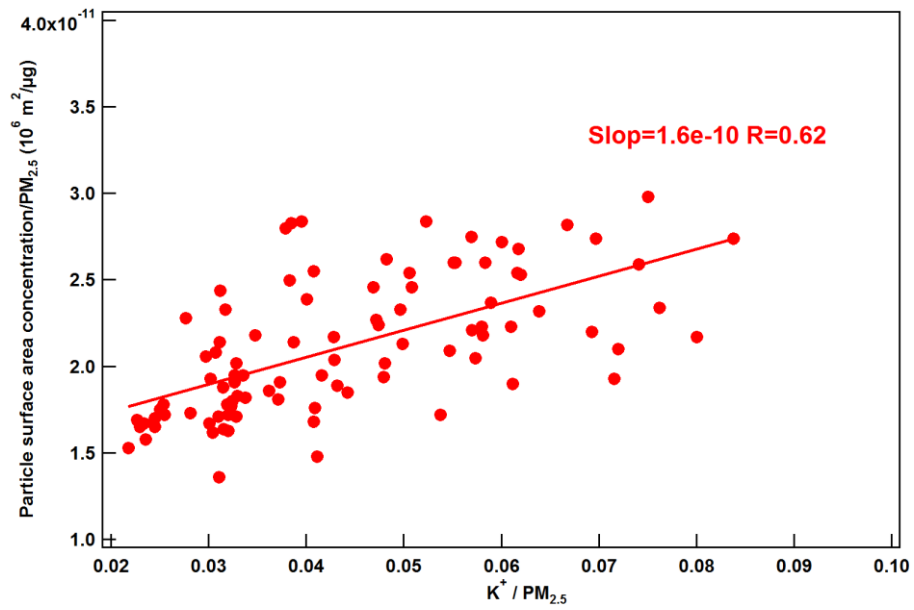


Fig. 8 Scatter plot between the ratio of particle surface area to PM_{2.5} and the abundance of potassium in PM_{2.5} for nighttime samples during BB during BB period.

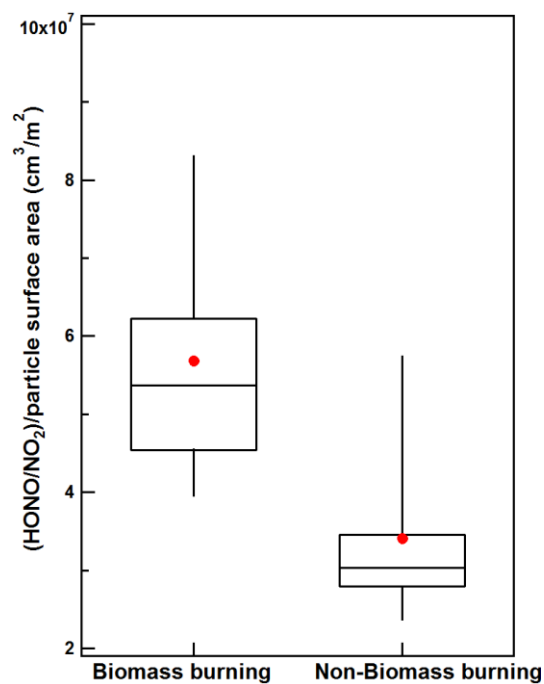


Fig. 9 Whisker plot of the ratios between HONO/NO₂ and particle surface area concentration for the balanced samples (02:00-05:59) with the particle surface area in the range of $1.5\text{--}2.2 \times 10^{-9} \text{ m}^2 \text{ cm}^{-3}$ during the BB (14 samples) and non-BB periods (21 samples).

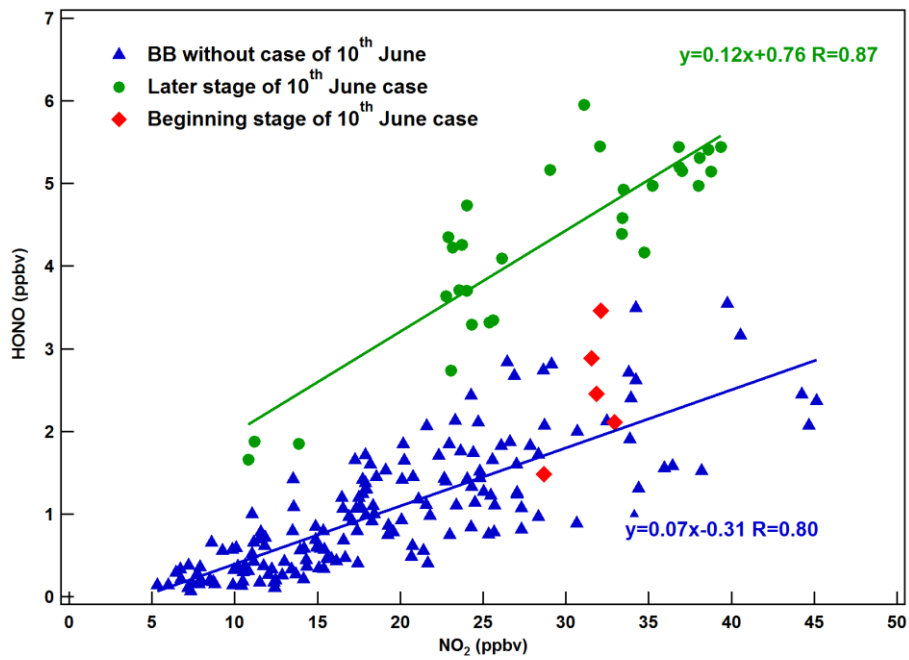


Fig. 10 Scatter plot between HONO and NO₂ concentration during the BB periods (without the case of 10th June, blue solid squares), the beginning (red solid diamonds) and latter (green dots) state of the June 10th episode.

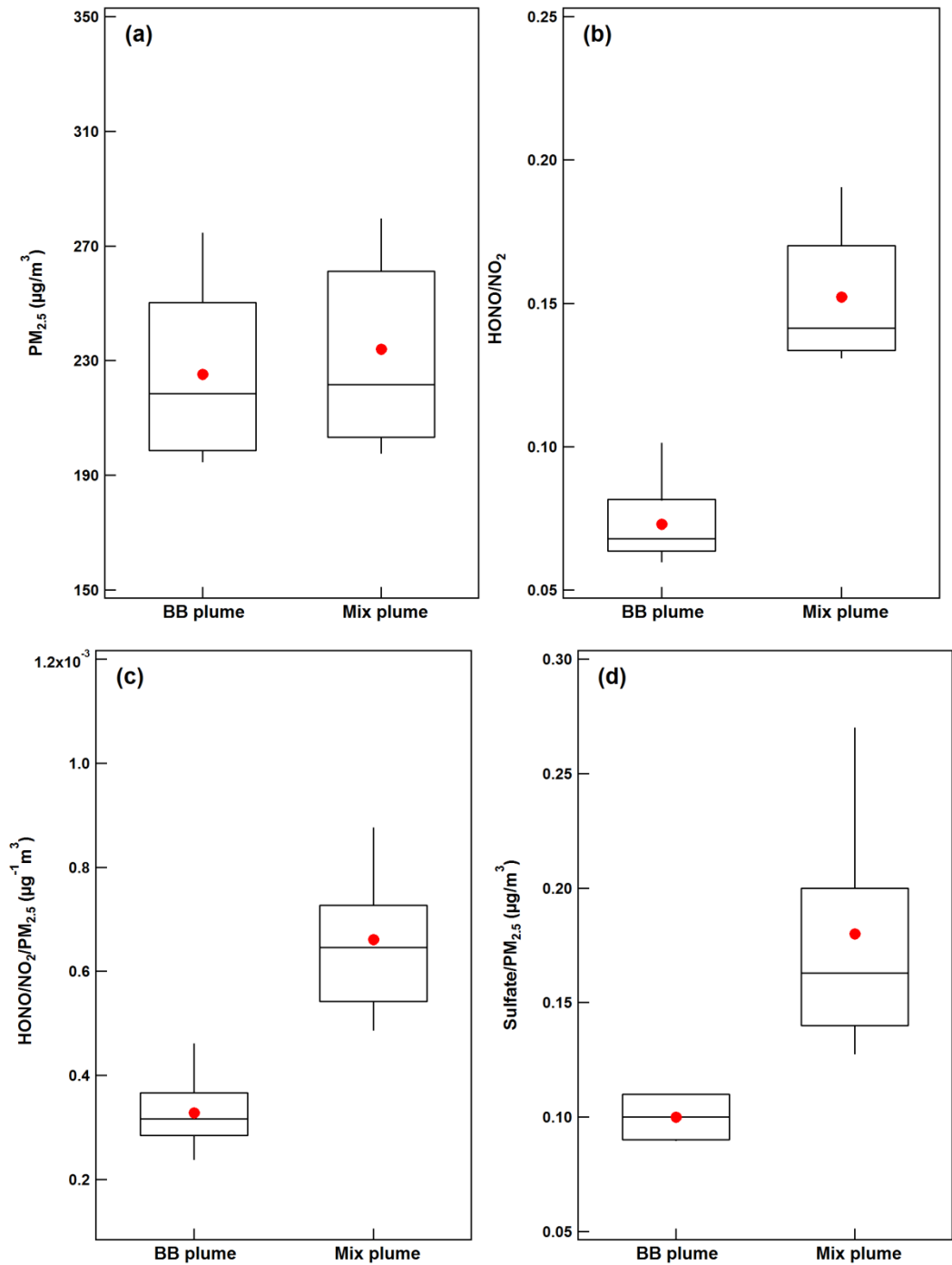


Fig. 11 Whisker plots of (a) $PM_{2.5}$ mass, (b) ratios of HONO to NO_2 , (c) ratios of HONO/ NO_2 to $PM_{2.5}$ mass, (d) ratios of sulfate to $PM_{2.5}$, in the selected $PM_{2.5}$ mass concentration range (190–300 $\mu\text{g m}^{-3}$) in BB plume (10 samples) and the mixed plume (27 samples).

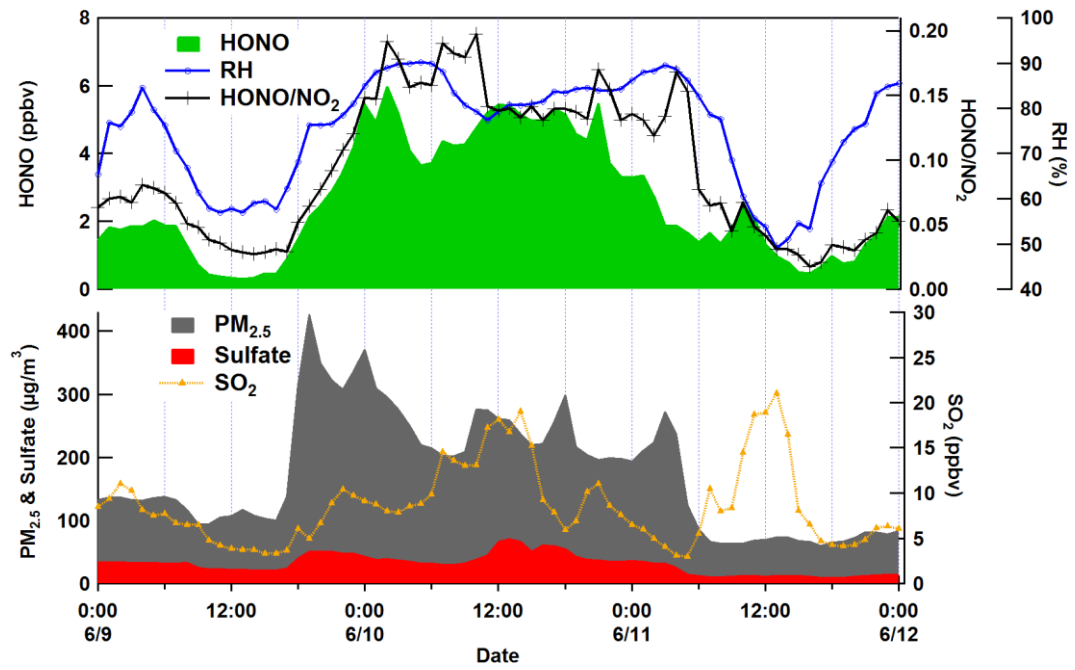


Fig. 12 Temporal variations of HONO, HONO/NO₂ ratios, RH, PM_{2.5}, sulfate in PM_{2.5} and SO₂ during 9 - 11 June 2012 at the SORPES central site.

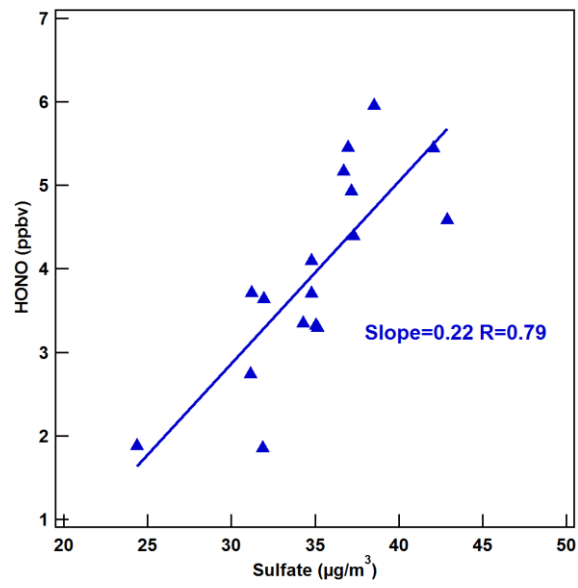


Fig. 13 Scatter plot between HONO and sulfate concentration in PM_{2.5} during the nighttime on 10 June